Separation and Purification Technology 231 (2020) 115899

Contents lists available at ScienceDirect

Separation and Purification Technology

journal homepage: www.elsevier.com/locate/seppur

Efficient separation of free organic liquid mixtures based on underliquid superlyophobic coconut shell coated meshes

Weimin Liu[a,1], Xiangge Bai[a,1], Yongqian Shen[b,*], Peng Mu[a], Yaoxia Yang[a], Jian Li[a,*]

[a] Research Center of Gansu Military and Civilian Integration Advanced Structural Materials, College of Chemistry and Chemical Engineering, Northwest Normal University, Lanzhou 730070, PR China

[b] State Key Laboratory of Advanced Processing and Recycling of Non-ferrous Metals, Key Laboratory of Nonferrous Metal Alloys and Processing, Ministry of Education, School of Materials Science & Engineering, Lanzhou University of Technology, Lanzhou 730050, PR China

ARTICLE INFO

Keywords:
Coconut shell
Hierarchical rough structure
Underliquid superlyophobicity
Organic liquids mixtures separation

ABSTRACT

The separation of multiphase liquid mixtures plays an important role in industrial production and environmental protection. The organic liquids (OLs) usually show approximate wettability on most of common materials owing to smaller surface tension. Therefore, the separation of OL mixtures is more difficult than the separation of oil/water mixtures. The current research on separation of OL mixtures is mainly through the covalent modification to precisely control the surface energy of materials, which is extremely complicated. Herein, a novel underliquid superlyophobic concept was presented for the separation of immiscible OL mixtures, which only depended on a relatively stable liquid-repellent interface. Furthermore, the minimum system's free energy principle was used to explain this wetting behavior. Compared with the previous reports, the work does not involve in various low surface energy substances, thus it is facile, eco-friendly and easily scale-up. Thus, the study provides a general strategy to separate the OL mixtures for the product purification and environmental protection.

1. Introduction

Materials with selective wettability have been widely used in the efficient separation of liquid mixtures, including the separation of oil/water mixtures and organic liquids (OLs) mixtures [1]. These complex liquid mixtures often need to be separated so that they can be purified, discharged harmlessly and resource recycling [2]. In the past decade, a large number of materials with superhydrophobicity or superhydrophilic/underwater superoleophobicity have been successfully prepared to separate oil/water mixtures, such as mesh-based materials [3–8], 3D porous foams [9–12], sand [13], and biomass materials [14,15] et al. However, a simple oil/water separation system cannot satisfy the requirements of complex liquid mixtures in practical industrial processes, especially in the chemical, medical and food industry. The separation of organic mixtures is crucial that not only prevents the secondary pollution, but also enhances the recycling of the organic liquids. Unfortunately, the separation of OLs mixtures is more difficult than the separation of oil and water because they show homogeneous wettability. In theory, to achieve the separation of OLs mixtures, the membrane must enjoy inverse wettability (lyophobicity and lyophilicity) for the mixture of two organic liquids. In other words, the membranes should show lyophobicity for one liquid and lyophilicity for another in the OLs mixtures. Recently, many materials can be used for the separation of OLs mixtures [16,17]. For example, Wang and cooperator successfully separated the immiscible OLs mixtures by modifying the surfaces with different silanes [17]. Liu et al. prepared the nanoneedle-covered copper mesh that was modificated with perfluorodecyltriethoxysilane (PFTS) for nonaqueous multiphase liquid separation [18]. The above mentioned materials are mostly through covalent modification to accurately regulate the materials' surface energy between the intrinsic wetting thresholds of two immiscible OLs, which can endow materials with superlyophobicity and superlyophilicity to achieve the OLs separation. Nevertheless, this approach suffers from inherent limitations such as complex operation, high cost and environmental unfriendly, which severely restrict its applicability. Besides, the low surface tension differences between OLs are also a great challenge for these material designs. Hence, how to prepare a material with low-cost, process simple and environmentally friendly for the separation of the OLs mixtures became a new trend.

Due to the surface tension of the OLs is much smaller than water, it shows the lyophilicity on the surface of most materials. Generally speaking, the wettability of the membrane was mainly determined by

* Corresponding authors.
E-mail addresses: syqch@163.com (Y. Shen), jianli83@126.com (J. Li).
[1] These authors contributed equally.

https://doi.org/10.1016/j.seppur.2019.115899
Received 2 July 2019; Received in revised form 4 August 2019; Accepted 4 August 2019
Available online 05 August 2019
1383-5866/

the surface roughness and the chemical composition of the surface [19,20]. According to Cassie's theory [21], the water-air-solid interface can be formed due to air molecules trapped on the surface of micro/nano rough structures. Based on the repulsion of air to water, water droplet can stay on the asperities surface [22]. The compound interface decreases the contact area of water and solid, which contributes greatly to the increase in hydrophobicity [23–25]. Inspired by the above reason, a novel underliquid superlyophobic strategy is presented for immiscible OLs mixtures separation by means of the pre-wetted with high surface tension.

The coconut shell is a typical green lignocellulosic biomass material, which contains a large number of biodegradable and non-toxic substances, such as glucan, xylan and so on. [26]. More importantly, the coconut shell contains a variety of chemical or functional groups such as acetamido, carboxyl and hydroxyl, etc., which endows the coconut shell superamphiphilicity. Moreover, the coconut shell is an agricultural waste produced in the process of production, and its treatment is an environmental problem. Therefore, it is promising that the coconut shell can be used as a material with underliquid superlyophobicity for immiscible OLs mixtures separation, which not only can relieve the pressure on the environment, but also become a good way to separate the mixtures of OLs. In this study, a coconut shell coated stainless steel mesh (CSCMs) with hierarchical rough structure was fabricated through a facile and easily scale-up spraying process. Lyophobic and lyophilic surfaces are highly dependent not only on surface energy but also on surface roughness. Thus, the hierarchical roughness improved both lyophilicity and lyophobicity significantly. The underliquid superlyophobic property can be easily implemented by introducing a high surface tension liquid ($liquid_1$) into the rough structure of the as-prepared CSCMs, forming a liquid-repellent interface to reject the immiscible low surface tension liquid ($liquid_2$). Well-matched solid and liquid surface energies as well as the roughness, ensure the stability of the liquid-repellent interface. In doing so, the as-prepared membrane could block permeation of $liquid_2$, but let $liquid_1$ pass through it, thus realizing successive separation of OLs mixtures. Compared with the previous report, the underliquid superlyophobic material does not depend on any low surface energy material to achieve superlyophobicity for one liquid and superlyophilicity for another. That is, this new separation strategy is facile, low cost and easily obtained, which does not need to precisely control the surface energy of the membranes to realize the separation of OLs mixtures. The approach was expected to become a competitive candidate for complex organic chemical product separation, resource recycling, and environmental protection.

2. Experimental

2.1. Materials

Waste coconut shell was obtained from a local fruit supplier in Lanzhou, China. The chemical compositions of the waste coconut shell were tested by the high performance liquid chromatograph (HPLC) system. The result showed that the hydrophilic substances in waste coconut shell were mainly glucan, xylan and klason-lignin, and their mass fractions were 29.30%, 25.92% and 24.36%, respectively. The stainless steel mesh (300 mesh size) was purchased from Anping Huirui wire mesh manufacturer, which was ultrasonicated in acetone and ethanol sequentially before use. Kerosene, diesel, hexane, heptane, petroleum ether, toluene, cyclohexane, formamide (FA), ethylene glycol (EG) and propylene glycol (PG) were purchased from Guangdong Guanghua Sci-Tech Co. Ltd. The surface tension is summarized in Table S1. All the organic solvents were analytical grade.

2.2. Pretreatment of the coconut shell

Firstly, the dirty waste coconut shells were cleaned by ultrasonic with deionized water, and then dried in the oven at 90 °C for 2 h. After that, the waste coconut shells were shattered by using high-speed multifunction grinder to obtain the crude coconut shell. The uniform powder is then collected through a 400-mesh standard screen.

2.3. Preparation of coconut shell-coated mesh

The aluminum phosphate (AP) binder was prepared by mixing Al $(OH)_3$ with orthophosphoric acid in a molar ratio of 1:3 under stirring at 100 °C for 3 h. 0.5 g coconut shell powder was dispersed in 15 mL of absolute ethanol to obtain mixture solution, and then 1 g AP binder was dissolved in 5 mL distilled water. Subsequently, the AP solution was added in the aforementioned coconut shell solution, which was stirred vigorously to obtain homogeneous solution. After that, the homogeneous solution was sprayed on stainless steel mesh substrate with 0.2 MPa compressed air gas. The distance between the spray gun and the substrate was about 15 cm. Finally, the CSCMs were heated treated at 120 °C for 2 h. to curing the CSCMs.

2.4. Separation of the immiscible OLs mixtures

The CSCMs was fixed between two Teflon fixtures, both of which were attached with glass tubes. In this study, seven types of oils and organic solvents were served as $liquid_2$, including kerosene, diesel, hexane, petroleum ether, heptane, cyclohexane, toluene. And the formamide, ethylene glycol and propylene glycol were served as $liquid_1$. The $liquid_2$ was colored with Oil red O and mixed with $liquid_1$ that was colored with methylene blue. Before separation, The CSCMs was completely pre-wetted by a small quantity of $liquid_1$. Then, immiscible OLs mixtures (volume ratio = 1:1) were poured onto the upper glass tube. The driving force was its own gravity during the separation process.

3. Characterization

Composition analysis (contents of glucan, xylan and Klasonlignin) was performed according to the NREL procedure [27]. The SH1011 column (Shodex) was installed into the high performance liquid chromatograph (HPLC) system (Waters 2698, USA) to determine the sugar concentrations at 50 °C. The flow rate of 5 mM H_2SO_4 used as the mobile phase was 0.5 mL/min. The morphological structures of the origin and as-prepared mesh surfaces were characterized by field emission scanning electron microscopy (FE-SEM, Zeiss). Specific surface and pore size distribution analyzer (AUTOSORB-1-MP, USA) was operated to characterize the CSCMs. Energy-dispersive spectrometry (EDS) spectra were collected on the Zeiss Ultra Plus equipped with an EDS detector (Oxford, Aztec-X-80). The values of liquid contact angles (CAs) and sliding angles (SAs) were measured with a SL200KB apparatus at ambient temperature by injecting 5 μL of liquid droplets on the coated meshes. The average CAs values were obtained by measuring the same sample in at least five different positions. Fourier transform infrared (FT-IR) spectroscopy was performed with a Bio-Rad FTS-165 instrument.

4. Results and discussion

The surface morphology of the original stainless steel mesh and the CSCMs were investigated by FE-SEM. As showed in Fig. 1a, the original mesh has an average pore diameter of about 50 μm (300 mesh size) and has a smooth surface (inset of Fig. 1a), which is used as substrate. After coated with coconut shell, it can be seen obviously that the origin stainless steel mesh surface was completely covered, which became rough with many irregularly distributed microparticles (Fig. 1b). The further magnified FE-SEM image in Fig. 1c shows that the surface of coconut shell was not smooth, there were a number of micro/nanoscale particles and debris of different sizes distribute randomly over a single

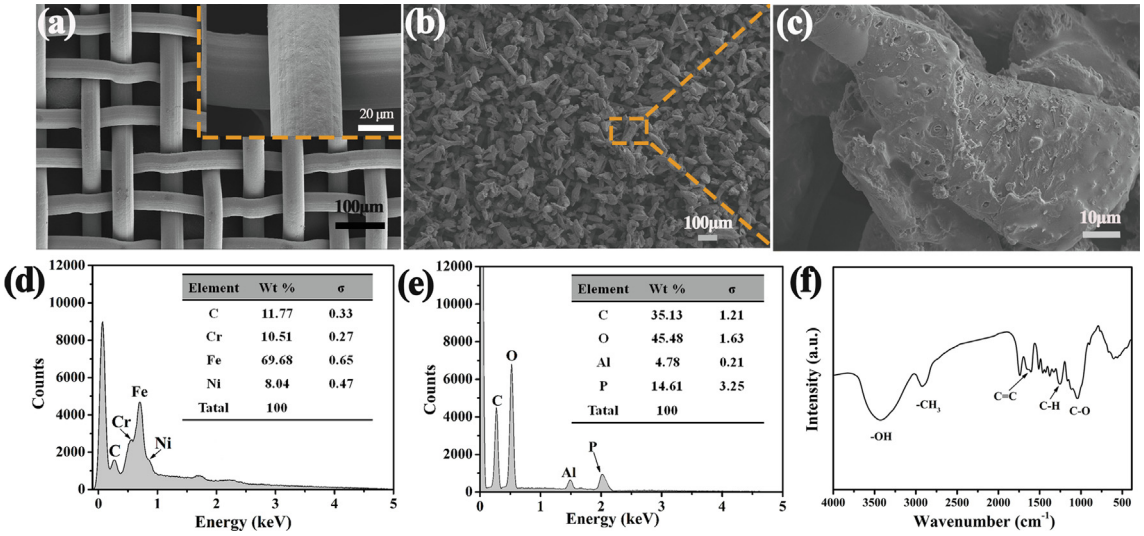

Fig. 1. FE-SEM images of (a) the original stainless steel mesh and (b and c) the CSCMs in different magnifications, respectively. The EDS results of (d) the original stainless steel mesh and (e) the CSCMs. (f) FT-IR spectrum of the CSCMs.

coconut shell surface. The hierarchical micro/nanoscale rough structure is crucial for forming stable underliquid (super)lyophobicity. Moreover, the pore size distribution of CSCMs was obtained by nitrogen sorption measurements [28] (Fig. S1). It can be seen that both mesopores (20–50 nm) and macropores (> 50 nm) are simultaneously existed in CSCMs. In addition, the surface chemical composition of origin stainless steel mesh and the CSCMs was measured by the EDS. Fig. 1d demonstrated that the C, Cr, Fe and Ni four elements in the spectra of the origin stainless steel mesh. After coated with the coconut shell, those above mentioned peak disappeared and replaced by others new spectra. There were new peaks appearing including O, Al and P elements in Fig. 1e. Combined with the element content of stainless steel mesh coated by coconut shell before and after (inset of Fig. 1d and e), the coconut shell was successfully loaded to the stainless steel mesh. This is due to coconut shell was a kind of biomass material, which contained abundant glucan, xylan and klason-lignin that were mainly made up of C and O elements. To further identify the element distribution of the CSCMs, element mapping were listed in Fig. S2. It can be seen that two mainly elements (C and O) were clearly observed on the surface of the CSCMs. The appearance of P and Al elements was due to the addition of AP binder. Moreover, the functional groups of coconut shell were characterized by the FT-IR spectra. As exhibited in Fig. 1f, a strong wide peak appeared at 3500–3400 cm^{-1}, suggesting the existence of hydroxyl groups in the CSCMs. The absorption peak at 2927 cm^{-1} arises from $-CH_3$ groups [29]. The peaks ranging from 1680 cm^{-1} to 1610 cm^{-1} corresponded to the stretching of the C=C bonds in the aromatic rings. The absorption peaks at 1300–1000 cm^{-1} could be accounted to angular deformation in the plane of the C—H bonds of aromatic rings and the peaks at 1200–1000 cm^{-1} matched the axial C-O bond in phenols [30]. The hierarchical micro/nanoscale rough structure and the chemical composition with polar group of the as-prepared CSCMs are indispensable for the underliquid (super)lyophobicity.

The wettability of the CSCMs was assessed comprehensively by measurement of the CAs and SAs. As exhibited in Fig. 2a, when FA and kerosene droplets contacted with the CSCMs, they were immediately spread out and permeated though the CSCMs with the CAs nearly 0°, which indicated that the CSCMs were superamphiphilic to two OLs in air. On the contrary, when the CSCMs was immersed into FA, oil droplet (kerosene) was like a small sphere, and the oil CAs was 155.7° (Fig. 2b), indicating the CSCMs.

presented an outstanding underliquid superlyophobic performance (Fig. 2c). For a series of oil CAs under FA and EG, as shown in Fig. 2f and g, the CAs of a series of oils droplet on the CSCMs were all larger than 150° and the SAs on the CSCMs were found to bthate less than 10°. Analogously, these liquid droplets CAs values are colse to 150° under PG in Fig. 2h, being very approaching to superlyophobic, which were due to the surface tension differences between PG and $liquid_1$ were quite small. In addition, the dynamic $liquid_2$-adhesion measurement was implemented to further testify the property of low adhesion under FA (Fig. S3). The SAs did not show for its high adhesion under PG. There is a noteworthy difference in CAs and SAs values of $liquid_2$ under different $liquid_1$, which the CAs and SAs are decrease and increase successively under FA, EG and PG, respectively. The Young's equation can be extended from the solid surface in air to a $liquid_2$ droplet on a solid surface in the $liquid_1$ to interpret the above phenomena. Thus, the formula (1) can be got from Young's equation to calculate the CAs of the $liquid_2$ in $liquid_1$–$liquid_2$–solid three-phase system [31]:

$$cos\theta_{L_1-L_2} = \frac{\gamma_{L_2-a}cos\theta_{L_2} - \gamma_{L_1-a}cos\theta_{L_1}}{\gamma_{L_2L_1}} \quad (1)$$

where γ_{L_1-a}, γ_{L_2-a} and $\gamma_{L_2-L_1}$are the $liquid_1$–air interface tension, $liquid_2$–air interface tension and $liquid_2$-$liquid_1$ interface tension, respectively. θ_{L_1}, θ_{L_2} and $\theta_{L_2-L_1}$ are the intrinsic CAs of $liquid_1$ in air, $liquid_2$ in air and $liquid_2$ under $liquid_1$, respectively. As can be seen from Eq. (1), the $cos\theta_{L_1-L_2}$ is always negative because the as-prepared CSCMs enjoys superlyophilic for $liquid_1$ and $liquid_2$ in air and the surface tension of $liquid_2$ is much lower than that of $liquid_1$. Combined with the Cassie theory and the high rough surface of the as-prepared CSCMs, the underliquid (super)lyophobicity can be well understood for $liquid_2$ under $liquid_1$. Furthermore, from Eq. (1), the CAs decrease with the decrease of the difference of surface tension between $liquid_2$ under $liquid_1$, which coincide with the experimental results (Fig. 2f–h). For the change of SAs, it depends on the adhesion of the $liquid_2$ on the solid surface under $liquid_1$. As exhibited in Fig. 2d, a droplet sits on the surface of solid with a low adhesion. In this case, the $liquid_2$-solid contact model is a discrete “point contact”, that is to say, the triple-phase contact line (TCL) is discontinuous. Therefore, in the process of moving forward and backward, there is little or no difference in energy between different states, so the droplets roll easily on the surface. When the CAs decrease with the decrease of the difference of surface tension between $liquid_1$ and $liquid_2$, the $liquid_2$ penetrates into the microroughness of solid. As a result, the contact model changes from discontinuity “point contact” to continuous “line contact” (Fig. 2e). Hence, the TCL has to overcome certain energy barriers before rolling, and this explains why the surface can have super-high adhesion [32,33]. In brief, the underliquid (super)

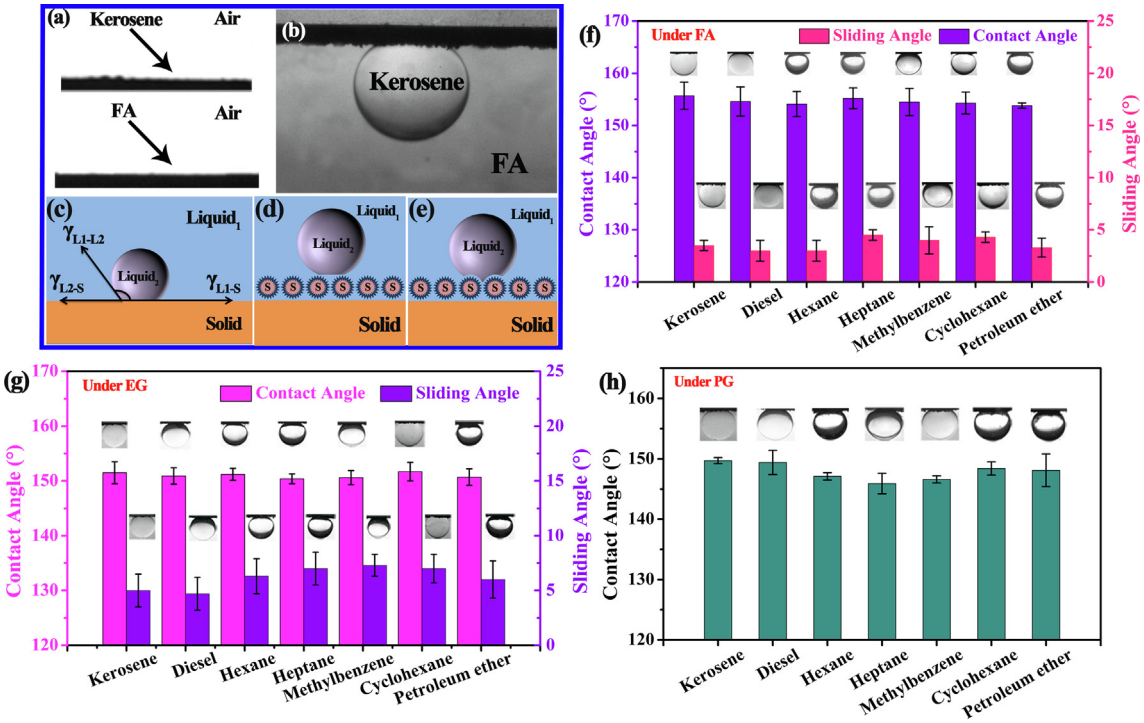

Fig. 2. (a and b) The wetting behavior of the CSCMs toward (c) Schematic illustration of liquid–solid contact mode in the liquid$_1$–liquid$_2$–solid three-phase system (d) low adhesion state (e) high adhesion state. (f–h) The CAs and SAs of various liquid$_1$ droplets under different liquid$_2$ medium on the CSCMs.

lyophobicity of the as-prepared CSCMs indicated that it has a good application prospects in the separation of immiscible OL mixtures.

To determine whether a solid will be wetted preferentially by a liquid$_1$ or liquid$_2$, the total interfacial energy of the individual wetting configurations was compared by the theoretical model (Fig. 3a). Configuration 1 and 2 refer to the state where the soild is completely wetted by liquid$_1$ and liquid$_2$, respectively. By comparing the energy states of configurations 1 and 2, one can determine the required solid/liquid combinations to form a stable film of liquid$_1$. E_1 and E_2 represent the total interfacial energies per unit area of the wetting configurations 1 and 2 respectively. In addition, γ_{s1}, γ_{s2}, γ_1 and γ_2 represent the surface energies of the solid-liquid$_1$ interface, solid-liquid$_2$ interface, liquid$_1$-vapor interface, and liquid$_2$-vapor interface, respectively. R represents the roughness factor of the solid, which is defined as the ratio between the actual and projected areas of the surface [34]. To find the conditions such that configuration 1 is always at a lower energy state than configuration 2, we have $\Delta E = E_1 - E_2 < 0$, which can be further expressed as,

$$\Delta E = R(\gamma_{s1} - \gamma_{s2}) + \gamma_1 - \gamma_2 < 0 \quad (2)$$

using the Young equation, we have

$$\Delta E = R(\gamma_2 cos\theta_2 - \gamma_1 cos\theta_1) + \gamma_1 - \gamma_2 < 0 \quad (3)$$

where θ_1, and θ_2 are the surface energy of the equilibrium contact angles of liquid$_1$ and liquid$_2$ on a flat solid surface, respectively. Satisfying above equation will ensure a stable liquid$_1$-repellent film formation. If the $\Delta E > 0$, the liquid$_1$ film will be replaced by the liquid$_2$. To verify the theoretical model, a number of different solid/liquid$_1$/

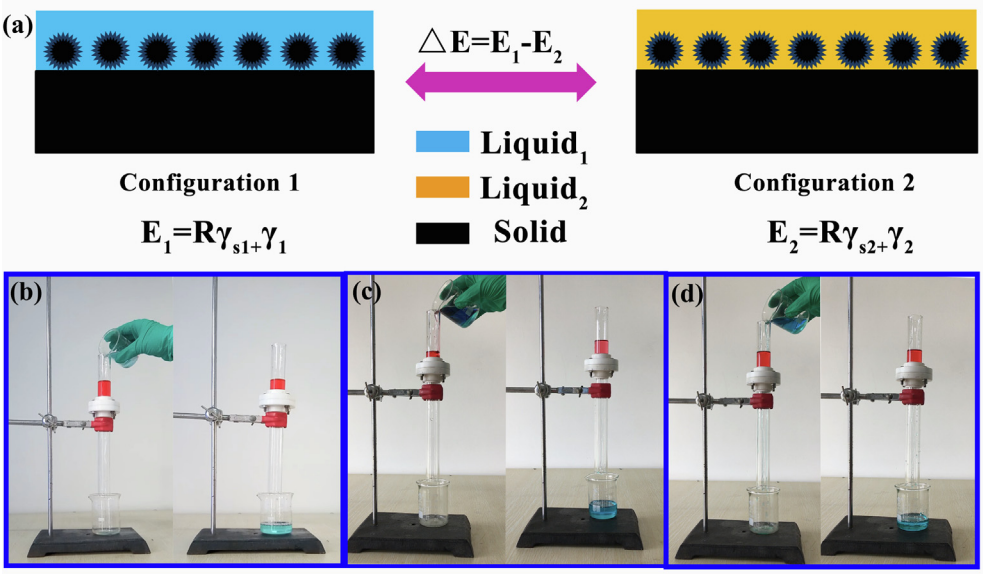

Fig. 3. (a) Theoretical model for maintaining a stable liquid film. (b–d) Separation process of FA/kerosene mixtures, EG/kerosene mixtures and PG/kerosene mixtures, respectively. (The FA, EG and PG are dyed with methylene blue and kerosene is dyed with Oil Red O in order to enhance the visual effect). (For interpretation of the references to colour in this figure legend, the reader is referred to the web version of this article.)

Table 1
Comparison of the governing relationships with experimental observations for various solid-liquid$_1$-liquid$_2$ combinations.

Liquid$_1$	Liquid$_2$	△E (mJ m^{-2})	Stable Film?	
			Theory	Exp.
FA	Kerosene	−14.67	Y	Y
	Diesel	−10.28	Y	Y
	Hexane	−20.91	Y	Y
	Petroleum ether	−20.86	Y	Y
	Heptane	−18.72	Y	Y
	Cyclohexane	−14.22	Y	Y
	Toluene	−9.14	Y	Y
EG	Kerosene	−22	Y	Y
	Diesel	−17.76	Y	Y
	Hexane	−28.33	Y	Y
	Petroleum ether	−28.22	Y	Y
	Heptane	−26.13	Y	Y
	Cyclohexane	−21.63	Y	Y
	Toluene	−16.55	Y	Y
PG	Kerosene	−12.79	Y	Y
	Diesel	−8.11	Y	Y
	Hexane	−19.12	Y	Y
	Petroleum ether	−19	Y	Y
	Heptane	−16.92	Y	Y
	Cyclohexane	−12.42	Y	Y
	Toluene	−7.34	Y	Y

Note: "Y" indicates that liquid$_1$ forms a stable liquid$_1$-repellent film, and does not get displaced by liquid$_2$.

liquid$_2$ combinations were explored and compared these results with the governing relationships. As presented in Table 1, these relationships agree favorably with all of the experimental conditions. It can be testified that the CSCMs preferentially captures the high surface tension liquid forming a relatively stable liquid$_1$-repellent interface, which repels the liquid$_2$ with a lower surface tension. Therefore, the CSCMs can make the liquids with high surface tension to pass through and hinder liquids with low surface tension, which does not need to choose different low surface energy silanes to accurately control the membranes' surface energy according to different OLs mixtures. Fig. 3b-d showed the separation process of the immiscible OLs mixtures on the CSCMs. We choose OLs mixtures of FA/kerosene (Fig. 3b), EG/kerosene (Fig. 3c) and PG/kerosene (Fig. 3d) to testify the separation capacity of the CSCMs. As presented in Fig. 3b, the FA/kerosene mixture was poured onto the pre-wetted CSCMs with FA, FA selectively permeated through the CSCMs and kerosene was intercepted and retained in the upper tube. After separation, there is no visible liquid mixture in the collected liquid, which can be separated effectively. Analogously, the other mixtures can be separated with the same method (Fig. 3c and d).

The robustness of the CSCMs is determined by the intrusion pressure, below which the CSCMs can work well. The experimental intrusion pressure of liquids flowing through the CSCMs was calculated by measuring the maximum height of oil that the CSCMs can support using Eq. (4):

$$\Delta P_{exp} = \rho g h_{max} \tag{4}$$

where ΔP_{exp} is the experimental intrusion pressure, ρ is the density of the liquid, g is the acceleration of gravity, and h_{max} is the maximum height of liquid the CSCMs can support. The intrusion pressures were measured for a serious of liquids, as exhibited Fig. 4. From left to right, the intrusion pressure of liquid$_2$ that FA pre-wetted mesh can support (Fig. 4a), EG pre-wetted mesh can support (Fig. 4b) and PG pre-wetted mesh can support (Fig. 4c), respectively. Meanwhile the theoretical intrusion pressure can be calculated by Eq. (5):

$$\Delta P_{theo} = -\frac{2\gamma_{L_1L_2}cos\theta}{d} \tag{5}$$

where ΔP_{theo} is the theory intrusion pressure, $\gamma_{L_1L_2}$ is the interfacial tension between liquid$_1$ and liquid$_2$, θ is the contact angle of liquid$_2$ on the coated surface which was just immersed in liquid$_1$, and d is the average pore diameter, which is calculated from the SEM image of the CSCMs. Although there were differences between the theoretical calculations and experimental values for a serious of liquids intrusion pressure, fluctuate within a certain margin of error, which showed great relevance. Therefore, the maximum height of a special liquid$_2$ is supported by the as-prepared CSCMs, which can be estimated by calculation. Moreover, it is important to note that in the actual separation, liquid has a minimum height (h_{min}). If the $h_{max} < h_{min}$, the separation may fail due to the intrusion pressure is too small. Thus, there is a minimum for h_{max}. When the $h_{max} > h_{min}$, the sepatation is meaningful and effective. Combine the Eqs. (4) and (5), we have

$$\gamma_{L_1L_2} > -\frac{h_{min}d\rho g}{2cos\theta} \tag{6}$$

Therefore, the surface tension difference of the two-phase organic liquid to be separated has a lower limit for the separation membrane with a specific pore size. The surface tension difference of the two-phase organic liquid to be separated can be further reduced by decreasing the aperture, but this is at the expense of decreased flux. Furthermore, the separation performance of the CSCMs can be characterized by the separation efficiency. To evaluate the separation efficiency of the CSCMs, it can be obtained by following Eq. (7):

$$R(\%) = \frac{V_a}{V_b} \times 100 \tag{7}$$

where R(%) is separation of the coated mesh, V_b and V_a are the volume of the lower surface tension liquid before and after the separation process, respectively. Fig. 5d exhibited the separation efficiency of the CSCMs, showing the high separation efficiency greater than 96% for various OLs mixtures. In addition, there are also presented the high separation efficiency for other OLs mixtures (Fig. S4). Furthermore, the flux is an indispensable parameter for practical operation, which values were calculated using Eq. (8):

$$F = \frac{V}{St} \tag{8}$$

where F is the flux, V is the volume of liquid$_1$ that permeates through the CSCMs, S is the effective area of the CSCMs, and t is the required time of a certain volume to pass through the CSCMs. As showed in Fig. 4e, the flux of FA was obviously higher (5.45 L m^{-2} s^{-1}) than that of EG and PG, which was due to the high viscosity of EG and PG. Furthermore, to further examine the separation capacity of the CSCMs, Fig. 4f showed the relationship between separation efficiency and recycle numbers by taking the FA/kerosene mixture as an example. It can be seen the separation efficiency was still greater than 96% after 50 cycle times. In each cycle before use the CSCMs was washed by passing through of absolute ethanol. Therefore, the as-prepared CSCMs with excellent recyclability was a promising material for the separation of the OLs.

To better understand the OLs mixtures separation mechanism of the as-prepared CSCMs, the wetting process is modeled on the assumption that the pores are arranged approximately in a regular square array (Fig. 5). When a wettable liquid contacts the membrane in air, it spreads instantly on the membrane under the action of the capillary force. According to the Eq. (5), due to the CSCMs shown the superamphiphilicity in air, θ is nearly 0°, the $\Delta p < 0$ and the CSCMs cannot support any pressure from the weight of the liquid in air (Fig. 5a). In contrast, when the CSCMs were pre-wetted by liquid$_1$, the liquid$_1$ can form a liquid$_1$-repellency layer in rough structures to repel liquid$_2$. The retention of liquid$_2$ above the CSCMs leads to $\theta > 90°$, thus the intrusion pressure$\Delta p > 0$, which means that the CSCMs can sustain pressure to some extent (Fig. 5b). The liquid$_2$ cannot permeate through the CSCMs spontaneously unless an external pressure is applied.

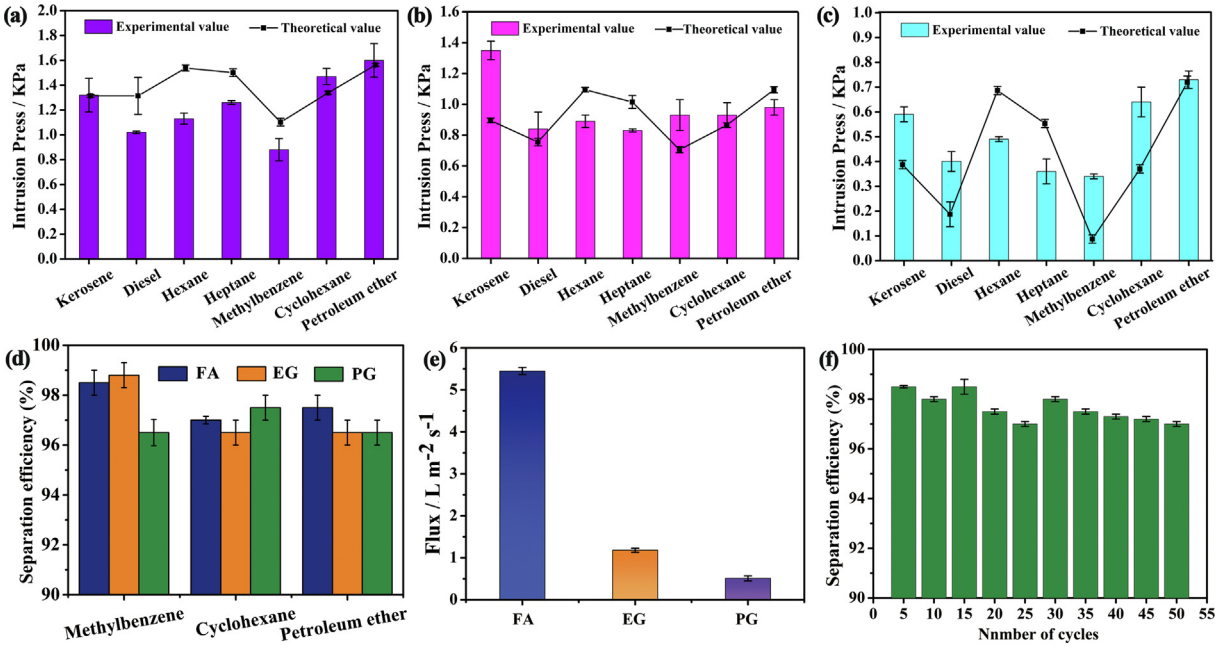

Fig. 4. The theoretical and experimental values of intrusion pressures for a series of mixtures under FA (a), under EG (b) and under PG (c), respectively. (d) The separation efficiency. (e) Flux of the coated meshes for FA, EG and PG. (f) The separation efficiency versus the recycle numbers by taking the FA/diesel mixture as an example.

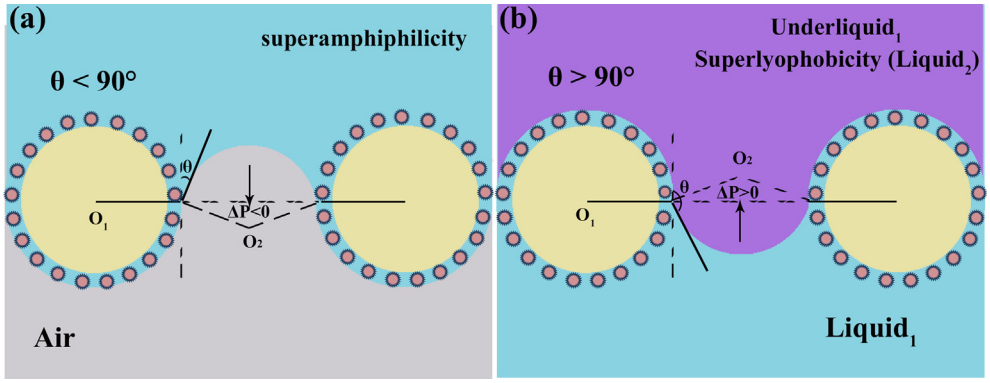

Fig. 5. Schematic diagram of the wetting mechanism of the as-prepared CSCMs. (a) $Liquid_1$ and $liquid_2$ will permeate through the CSCMs in air, because $\triangle P < 0$. (b) $Liquid_2$ can stay above the coated mesh CSCMs after pre-wetting by $liquid_1$, because $\triangle P > 0$. O_1 is the cross section center of the mesh and O_2 is the center of the spherical cap of the meniscus.

Table 2
Comparison of various superwettable materials for immiscible organic liquid mixtures separation.

Materials	Method	Superwettability	low surface energy materials	Flux ($L\,m^{-2}\,s^{-1}$)	Separation efficiency (%)	Refs.
$Cu(OH)_2$ nanoneedles mesh	Surface oxidation process	Superlyophobicity in air	Yes	33	97	18
Stainless steel meshes	Electrochemical etching	Lydrophobicity in air	Yes	–	> 94	35
Nanofibrous membranes	Electrospinning	Superlyophobicity in air	Yes	–	97	2
Copper oxide nanoneedle mesh	Oxidation and surface modification	Lydrophobicity in air	Yes	–	98	36
PVP nanofibrous membranes	Electrospinning	Superlyophobicity in air	Yes	0.27	99	16
Coconut shell coated mesh	Spraying	Underliquid Superlyophobic	No	5.45	> 96	This work

Note: "Yes" indicates that the material is involved into the low-surface energy substance.

Compared with previous materials [2,16,18,35,36], the separation method does not need to accurately control the membranes' surface energy according to different OL mixtures, which is facile and low cost (Table 2). From the above discussed, it is clear that the $liquid_1$ pre-wetted mesh allows the $liquid_1$ to permeate quickly, while the $liquid_2$ is rejected above the mesh, achieving effective separation of immiscible OLs mixtures.

5. Conclusion

In summary, a novel underliquid superlyophobic concept was presented for the separation of immiscible OL mixtures. The underliquid superlyophobicity was realized by introducing a high surface tension liquid ($liquid_1$) into the rough structure of the as-prepared CSCMs, forming a $liquid_1$-repellent interface to repel the immiscible low surface tension liquid ($liquid_2$). The pre-wetting CSCMs by $liquid_1$ allows the passage of high surface tension liquid and blocks the permeation of low

surface tension liquid, which achieved successive high-efficiency separation of OLs mixtures. Different from the study of previous for the separation of OLs mixtures, the approach avoided using many low surface energy materials, complex preparation processes, expensive drugs, and so on, which was simple, economical and environmentally friendly. This strategy will open new perspectives to separate multiphase liquid in product purification and environmental protection.

Acknowledgements

This project was funded by the National Natural Science Foundation of China (no. 5187021715), the Fok Ying-Tong Education Foundation of China (161044), the Natural Science Foundation for Distinguished Young Scholars of Gansu Province, China (18JR3RA083), China Postdoctoral Science Foundation (2018T110025, 2017M610031), and the Yong Teacher Research Group Foundation of Northwest Normal University (NWNULKQN-16-6). We also thank the Gansu International Scientific and Technological Cooperation Base of Water-Retention Chemical Functional Materials for financial support.

Appendix A. Supplementary material

Supplementary data to this article can be found online at https://doi.org/10.1016/j.seppur.2019.115899.

References

[1] X. Dong, J. Chen, Y. Ma, J. Wang, M.B. Chan-Park, X. Liu, L. Wang, W. Huang, P. Chen, Superhydrophobic and superoleophilic hybrid foam of graphene and carbon nanotube for selective removal of oils or organic solvents from the surface of water, Chem. Commun. 48 (2012) 10660–10662.
[2] L. Hou, L. Wang, N. Wang, F. Guo, J. Liu, Y. Chen, J. Liu, Y. Zhao, L. Jiang, Separation of organic liquid mixture by flexible nanofibrous membranes with precisely tunable wettability, NPG Asia Mater. 8 (2016) e334.
[3] Q. Zhang, Y. Cao, N. Liu, W. Zhang, Y. Chen, X. Lin, Y. Wei, L. Feng, L. Jiang, Recycling of PE glove waste as highly valuable products for efficient separation of oil-based contaminants from water, J. Mater. Chem. A 4 (2016) 18128–18133.
[4] L. Feng, Z. Zhang, Z. Mai, Y. Ma, B. Liu, L. Jiang, D. Zhu, A super-hydrophobic and super-oleophilic coating mesh film for the separation of oil and water, Angew. Chem. Int. Ed. 43 (2004) 2012–2014.
[5] Y. Long, Y. Shen, H. Tian, Y. Yang, H. Feng, J. Li, Superwettable coprinus comatus coated membranes used toward the controllable separation of emulsified oil/water mixtures, J. Membr. Sci. 565 (2018) 85–94.
[6] X. Wang, M. Li, Y. Shen, Y. Yang, H. Feng, J. Li, Facile preparation of loess-coated membranes for multifunctional surfactant-stabilized oil-in-water emulsion separation, Green Chem. 21 (2019) 3190–3199.
[7] J. Wang, F. Han, Y. Chen, H. Wang, A pair of MnO_2 nanocrystal coatings with inverse wettability on metal meshes for efficient oil/water separation, Sep. Purif. Technol. 209 (2019) 119–127.
[8] H. Kang, Z. Cheng, H. Lai, H. Ma, Y. Liu, X. Mai, Y. Wang, Q. Shao, L. Xiang, X. Guo, Z. Guo, Superlyophobic anti-corrosive and self-cleaning titania robust mesh membrane with enhanced oil/water separation, Sep. Purif. Technol. 201 (2018) 193–204.
[9] H. Bi, X. Huang, X. Wu, X. Cao, C. Tan, Z. Yin, X. Lu, L. Sun, H. Zhang, Carbon microbelt aerogel prepared by waste paper: an efficient and recyclable sorbent for oils and organic solvents, Small 10 (2014) 3544–3550.
[10] A. Halim, Y. Xu, K.-H. Lin, M. Kobayashi, M. Kajiyama, T. Enomae, Fabrication of cellulose nanofiber-deposited cellulose sponge as an oil-water separation membrane, Sep. Purif. Technol. 224 (2019) 322–331.
[11] H. Zhang, S. Lyu, X. Zhou, H. Gu, C. Ma, C. Wang, T. Ding, Q. Shao, H. Liu, Z. Guo, Super light 3D hierarchical nanocellulose aerogel foam with superior oil adsorption, J. Colloid Interface Sci. 536 (2019) 245–251.
[12] Z. Li, B. Wang, X. Qin, Y. Wang, C. Liu, Q. Shao, N. Wang, J. Zhang, Z. Wang, C. Shen, Z. Guo, Superhydrophobic/superoleophilic polycarbonate/carbon nanotubes porous monolith for selective oil adsorption from water, ACS Sustain. Chem. Eng. 6 (2018) 13747–13755.
[13] J. Li, C. Xu, C. Guo, H. Tian, F. Zha, L. Guo, Underoil superhydrophilic desert sand layer for efficient gravity-directed water-in-oil emulsions separation with high flux, J. Mater. Chem. A 6 (2018) 223–230.
[14] S. Sun, L. Zhu, X. Liu, L. Wu, K. Dai, C. Liu, C. Shen, X. Guo, G. Zheng, Z. Guo, Superhydrophobic shish-kebab membrane with self-cleaning and oil/water separation properties, ACS Sustain. Chem. Eng. 6 (2018) 9866–9875.
[15] H. Zhang, Y. Shen, M. Li, G. Zhu, H. Feng, J. Li, Egg shell powders-coated membrane for surfactant-stabilized crude oil-in-water emulsions efficient separation, ACS Sustain. Chem. Eng. 7 (2019) 10880–10887.
[16] L. Wang, Y. Zhao, Y. Tian, L. Jiang, A general strategy for the separation of immiscible organic liquids by manipulating the surface tensions of nanofibrous membranes, Angew. Chem. Int. Ed. 54 (2015) 14732–14737.
[17] Y. Wang, J. Di, L. Wang, X. Li, N. Wang, B. Wang, Y. Tian, L. Jiang, J. Yu, Infused-liquid-switchable porous nanofibrous membranes for multiphase liquid separation, Nat. Commun. 8 (2017) 575.
[18] J. Liu, L. Wang, N. Wang, F. Guo, L. Hou, Y. Chen, J. Liu, Y. Zhao, L. Jiang, A robust $Cu(OH)_2$ nanoneedles mesh with tunable wettability for nonaqueous multiphase liquid separation, Small 13 (2017) 1600499.
[19] B. Wang, W. Liang, Z. Guo, W. Liu, Biomimetic super-lyophobic and super-lyophilic materials applied for oil/water separation: a new strategy beyond nature, Chem. Soc. Rev. 44 (2015) 336–361.
[20] X. Li, M. Cao, H. Shan, F. Handan Tezel, B. Li, Facile and scalable fabrication of superhydrophobic and superoleophilic PDMS-co-PMHS coating on porous substrates for highly effective oil/water separation, Chem. Eng. J. 358 (2019) 1101–1113.
[21] S.B.A.B.D. Cassie, Wettability of porous surfaces, Trans. Faraday Soc. 40 (1944) 546–551.
[22] X. Tian, V. Jokinen, J. Li, J. Sainio, R.H. Ras, Unusual dual superlyophobic surfaces in oil-water systems: the design principles, Adv. Mater. 28 (2016) 10652–10658.
[23] Z. Xue, S. Wang, L. Lin, L. Chen, M. Liu, L. Feng, L. Jiang, A novel superhydrophilic and underwater superoleophobic hydrogel-coated mesh for oil/water separation, Adv. Mater. 23 (2011) 4270–4273.
[24] S. Wang, L. Jiang, Definition of superhydrophobic states, Adv. Mater. 19 (2007) 3423–3424.
[25] J. Wang, F. Han, S. Zhang, Durably superhydrophobic textile based on fly ash coating for oil/water separation and selective oil removal from water, Sep. Purif. Technol. 164 (2016) 138–145.
[26] J. Li, C. Xu, Y. Zhang, X. Tang, W. Qi, Q. Wang, Gravity-directed separation of both immiscible and emulsified oil/water mixtures utilizing coconut shell layer, J. Colloid Interface Sci. 511 (2018) 233–242.
[27] U. Moilanen, E. Winquist, T. Mattila, A. Hatakka, T. Eerikäinen, Production of manganese peroxidase and laccase in a solid-state bioreactor and modeling of enzyme production kinetics, Bioprocess Biosyst. Eng. 38 (2015) 57–68.
[28] Y. Qian, Y. Yuan, H. Wang, H. Liu, J. Zhang, S. Shi, Z. Guo, N. Wang, Highly efficient uranium adsorption by salicylaldoxime/polydopamine graphene oxide nanocomposites, J. Mater. Chem. A 6 (2018) 24676–24685.
[29] O. Arslan, Z. Aytac, T. Uyar, Superhydrophobic, hybrid, electrospun cellulose acetate nanofibrous mats for oil/water separation by tailored surface modification, ACS Appl. Mater. Interfaces 8 (2016) 19747–19754.
[30] R. Mallampati, L. Xuanjun, A. Adin, S. Valiyaveettil, Fruit peels as efficient renewable adsorbents for removal of dissolved heavy metals and dyes from water, ACS Sustain. Chem. Eng. 3 (2015) 1117–1124.
[31] Y. Wang, C. Lai, X. Wang, Y. Liu, H. Hu, Y. Guo, K. Ma, B. Fei, J.H. Xin, Beads-on-string structured nanofibers for smart and reversible oil/water separation with outstanding antifouling property, ACS Appl. Mater. Interfaces 8 (2016) 25612–25620.
[32] M. Liu, L. Jiang, Switchable adhesion on liquid/solid interfaces, Adv. Funct. Mater. 20 (2010) 3753–3764.
[33] X.J. Huang, D.H. Kim, M. Im, J.H. Lee, J.B. Yoon, Y.K. Choi, "Lock-and-key" geometry effect of patterned surfaces: wettability and switching of adhesive force, Small 5 (2009) 90–94.
[34] T.S. Wong, S.H. Kang, S.K. Tang, E.J. Smythe, B.D. Hatton, A. Grinthal, J. Aizenberg, Bioinspired self-repairing slippery surfaces with pressure-stable omniphobicity, Nature 477 (2011) 443–447.
[35] A. Kim, C. Lee, J. Kim, Durable, scalable, and tunable omniphobicity on stainless steel mesh for separation of low surface tension liquid mixtures, Surf. Coat. Tech. 344 (2018) 394–401.
[36] M. Qiu, N. Wang, Z. Cui, J. Liu, L. Hou, J. Liu, R. Hu, H. Zhang, Y. Zhao, Evolution of copper oxide nanoneedle mesh with subtle regulated lyophobicity for high efficiency liquid separation, J. Mater. Chem. A 6 (2018) 817–822.